Earth and Planetary Science Letters 291 (2010) 1–9

Contents lists available at ScienceDirect

Earth and Planetary Science Letters

journal homepage: www.elsevier.com/locate/epsl

Partitioning of Mo, P and other siderophile elements (Cu, Ga, Sn, Ni, Co, Cr, Mn, V, and W) between metal and silicate melt as a function of temperature and silicate melt composition

K. Righter [a,*], K.M. Pando [a,b,d], L. Danielson [a,e], Cin-Ty Lee [c]

[a] NASA Johnson Space Center, Houston, Texas, United States
[b] Lunar and Planetary Institute, Houston, Texas, United States
[c] Dept. of Earth Sciences, Rice University, Houston, Texas, United States
[d] Mailcode JE23, ESCG Hamilton Sunstrund, NASA Johnson Space Center, 2101 NASA Pkwy., Houston, TX 77058, United States
[e] Mailcode JE23, ESCG Jacobs Technology, NASA Johnson Space Center, 2101 NASA Pkwy., Houston, TX 77058, United States

ARTICLE INFO

Article history:
Received 13 May 2009
Received in revised form 11 November 2009
Accepted 8 December 2009
Available online 25 January 2010

Editor: R.W. Carlson

Keywords:
siderophile
core
metal
mantle
partitioning

ABSTRACT

Metal–silicate partition coefficients can provide information about the earliest differentiation histories of terrestrial planets and asteroids. Systematic studies of the effects of key parameters such as temperature and melt composition are lacking for many elements. In particular, data for Mo is scarce, but given its refractory nature, is of great value in interpreting metal–silicate equilibrium. Two series of experiments have been carried out to study Mo and P partitioning between Fe metallic liquid and basaltic to peridotitic silicate melt, at 1 GPa and temperatures between 1500 and 1900 °C. Because the silicate melt utilized was natural basalt, there are also measurable quantities of 9 other siderophile elements (Ni, Co, W, Sn, Cu, Mn, V, Cr, Ga and Zn). The Ni and Co data can be used to assess consistency with previous studies. In addition, the new data also allow a first systematic look at the temperature dependence of Cu, Ga, Sn, Cr, Mn V and W for basaltic to peridotitic melts. Many elements exhibit an increase in siderophile behavior at higher temperature, contrary to popular belief, but consistent with predictions from thermodynamics. Using these new data we examine $D_{Mo}^{met/sil}$ and $D_{P}^{met/sil}$ in detail and show that increasing temperature causes a decrease in the former and an increase in the latter, whereas both increase with MgO content of the silicate melt. The depletions of Mo and P in the mantle of the Earth can be explained by metal–silicate equilibrium at magma ocean conditions — both elements are satisfied at *PT* conditions of an intermediate depth magma ocean for the Earth 22.5 GPa and 2400 °C.

Published by Elsevier B.V.

1. Introduction

Details of how the terrestrial planets formed and differentiated have remained elusive to planetary scientists. One hypothesis is that early in the Earth's formation, there was a magma ocean present (Li and Agee, 1996), and metallic liquid separated through the silicate liquid to form the metal core (Walter et al., 2000; Righter, 2003; Rubie et al., 2003). This scenario is based on studies of the metal–silicate partitioning of siderophile elements such as Ni, Co, W and Cr. There is debate about whether the magma ocean was shallow (e.g. 20–25 GPa and ~2000 °C; Li and Agee, 1996; Righter et al., 1997; Ohtani et al., 1997) or deep (e.g., 30–50 GPa and 3000–4000 °C; Wade and Wood, 2001; Chabot et al., 2005), yet there are aspects of the modeling and database that have not been fully explored. For example, the partitioning of many elements has not been studied systematically as a function of temperature. Although increasing temperature is generally expected to cause a decrease in metal–silicate partition coefficients ($D_{M/S}$), experimental data actually suggest otherwise in many cases where temperature causes an increase in $D_{M/S}$ (Capobianco et al., 1993). In addition, the effect of melt composition is known to be important for some elements, but most experimental studies have been carried out with basaltic silicate melts instead of the peridotitic melts expected in a magma ocean.

P and Mo are moderately siderophile elements that have sizable depletions in the mantle (Walter et al., 2000), but there have not been systematic studies of either in terms of temperature and melt composition. In addition, the natural samples used in the study contain trace amounts of additional siderophile elements which allows determination of partition coefficients for Ni, Co, W, Mn, V, Cr, Ga, Zn, Cu, Sn in addition to Mo and P. The results from these new experiments will be used to evaluate the conditions that may have prevailed during core formation in the early Earth.

* Corresponding author.
E-mail address: kevin.righter-1@nasa.gov (K. Righter).

0012-821X/$ – see front matter. Published by Elsevier B.V.
doi:10.1016/j.epsl.2009.12.018

2. Methods

2.1. Experimental

Experiments at 1.0 GPa and variable temperature high pressures were conducted using a non end-loaded piston cylinder apparatus at NASA-JSC. Experimental details of pressure, temperature and the assemblies were presented in Filiberto et al. (2008) and Righter et al. (2006). The sample used in this series of experiments was composed of 70 wt.% Knippa Basalt, the composition of which is described in Lewis et al. (1993), 29 wt.% Fe and 1 wt.% MoO_3. These were ground to a powder and mechanically mixed. Two types of capsules were used: graphite and polycrystalline MgO. Once samples were under pressure, they were heated to silicate superliquidus temperatures. Run durations were chosen based on equilibration times from previous experiments (Li and Agee, 1996; Righter et al., 1997), and also four experiments which formed a time series (see supplementary information Fig. S1). The samples were then power quenched to a silicate glass which contained large metallic liquid spheres (Fig. 1). The two different temperature series consisted of nine experiments at temperatures from 1500 to 1900 °C (Table 1).

2.2. Analytical

Glasses and metals from the run products were analyzed with an electron microprobe for major elements with a CAMECA SX100 electron microprobe, using an accelerating voltage of 20 kV and sample current of 20 to 40 nA (see additional details in Righter et al., 2009). Multiphase quenched silicate melt and metallic melt were analyzed by rastering the beam over a 10×10 μm area, for 20 to 50 different regions that were then averaged. Traverses from capsule wall to metal sphere show no variation in composition. Typical uncertainty for major elements analyzed by the NASA-JSC electron microprobe is <2%, and for Mo and P in metals <5%.

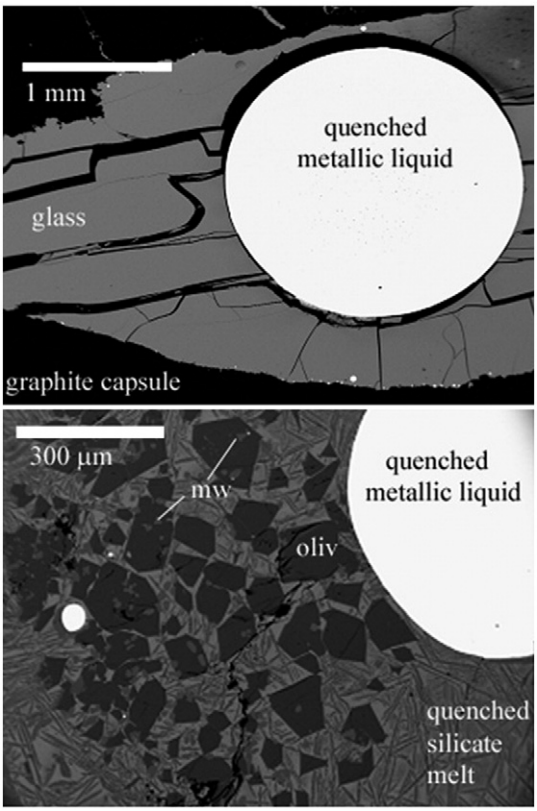

Fig. 1. Back scattered electron images of two experimental run products. Top: cow 25 showing graphite capsule (black), silicate glass (grey) and metal blobs (white); bottom: cow 12 showing silicate glass with dark olivine and light magnesiowüstite crystals (grey) and metal blobs (white).

Experiments cow 1, cow 3, cow 8, cow 20, and cow 28 used graphite capsules, causing the metallic liquid spheres to be C saturated. Carbon contents of metals were analyzed using a set of C-bearing steel standards with C contents between 0.08 and 2.78 wt.% C (BCS 152/3, 402 and 234/8 and LECO 501–504 and 501–505). Analysis was done with a PC2 crystal in differential mode counting for 20 s, and samples were not carbon coated, but instead a strip of carbon tape was used from holder frame to the metal sample edge.

Analyses of minor and trace elements (P, V, Cr, Mn, Co, Ni, Cu, Zn, Ga, Ge, Mo, Sn and W) were done by laser ablation inductively coupled plasma mass spectrometry (ICP-MS) at Rice University using ThermoFinnigan Element 2 ICP-MS coupled to a New Wave 213 nm laser ablation system (Agrinier and Lee, 2007). Analyses of minor and trace elements (P, V, Cr, Mn, Co, Ni, Cu, Zn, Ga, Ge, Mo, Sn and W) were done by laser ablation inductively coupled plasma mass spectrometry (ICP-MS) at Rice University using ThermoFinnigan Element 2 ICP-MS coupled to a New Wave 213 nm laser ablation system (Agrinier and Lee, 2007). Analyses were performed in medium mass resolution ($m/\Delta m = 3500$) in order to resolve all major isobaric molecular interferences. Isotopes analyzed were ^{30}Si, ^{31}P, ^{51}V, ^{52}Cr, ^{55}Mn, ^{57}Fe, ^{59}Co, ^{60}Ni, ^{63}Cu, ^{66}Zn, ^{69}Ga, ^{73}Ge, ^{74}Ge, ^{94}Mo, ^{95}Mo, ^{118}Sn, and ^{182}W (Tables 1 and 2). Measurements of several isotopes of the same element, such as for Ge and Mo, were conducted for additional assurance that interferences were not a problem. Drift of mass calibration was corrected for by centering on $^{40}Ar^{40}Ar^{+}$ dimer in each measurement. Laser was set at 10 Hz pulse frequency and an energy density of 10 mJ/cm^2. Measurements consisted of about 10 analyses of gas flow background followed by 40–50 measurements of the ablation signal. Gas background was averaged and then subtracted from ablation signal. Background-corrected signals were converted to concentrations using a combination of internal and external standards. ^{57}Fe was used as an internal standard for quenched metallic liquids and ^{25}Mg for glasses and quenched silicate liquids. Hoba and Filomena iron meteorites were used as external standards for the metals (Campbell and Humayun, 2005) while USGS basaltic glass standards (BHVO2g, BCR2g, and BIR1g) were used for the silicate glasses (Gao et al., 2002). Finally, limit of detection for each analysis was estimated at 3 times the standard deviation of the background divided by the sensitivity of the instrument as monitored by ^{25}Mg (see also Agrinier and Lee, 2007), and uncertainties are typically ~5% of the amount present (1σ). For partition coefficients, this corresponds to a typical uncertainty of 10% on the reported values of the partition coefficient; these are the error bars presented in the figures.

Although MnO is measured by EMPA, the Mn concentration data from LA-ICP-MS is used to calculate partition coefficients for Mn because of the greater precision and to avoid the correction of Mn and Fe interference with the EMPA data.

3. Results

3.1. Equilibrium

Several lines of evidence can be used to assess whether equilibrium was approached in these experiments. First, experiments cow 10 and 12 (using MgO capsules) crystallized olivine during the experiment and the composition of the olivine and coexisting melt can be used to assess whether equilibrium was approached in the experiments. Olivine-melt K_D are consistent with equilibrium: calculated Fo contents (X_{Fo}) based on a comprehensive olivine-melt K_D(Mg–Fe) model (Toplis, 2005) are within 0.01 of the measured olivine composition for each run (Table S1). Second, if the reaction of metal with silicate did not reach completion or equilibrium, there will be variable silicate compositions according to the equilibrium 2Fe +

Table 1
Summary table of all experimental conditions and silicate melt composition; all at 1.0 GPa.

Sample	Cow 10	Cow 12	Cow 17	Cow 16	Cow 1	Cow 3	Cow 8	Cow 20	Cow 28	Cow 25	Cow 24	Cow 3	Cow 22
T (°C)	1500	1600	1700	1800	1500	1600	1700	1800	1900	1600	1600	1600	1600
Dur. (min)	180	90	45	15	180	90	45	15	10	30	60	90	120
Capsule	MgO	MgO	MgO	MgO	C	C	C	C	C	C	C	C	C
fO_2	−1.60	−1.76	−1.76	−1.81	−1.44	−1.48	−1.45	−1.44	−1.56				
Phases	lm, ol, gl	lm, ol, mw, gl	lm, gl	lm, gl	lm, gl	lm, gl	lm, gl	lm, gl	lm, gl	lm, gl	lm, gl	lm, gl	lm, gl
SiO_2	30.2	31.4	32.1	32.6	39.2	39.2	37.8	38.1	38.6	38.8	38.8	39.2	39.3
TiO_2	4.39	3.71	3.36	2.80	3.42	3.28	3.36	3.28	3.11	3.19	3.02	3.28	3.02
Al_2O_3	11.2	10.9	10.0	9.0	10.3	10.9	12.1	10.2	11.5	10.2	8.7	10.9	10.2
FeO	15.35	11.49	11.42	11.36	17.08	16.55	17.03	17.12	17.2	16.23	15.64	16.55	15.57
MnO	0.18	0.15	0.15	0.14	0.21	0.20	0.21	0.19	0.19	0.19	0.20	0.20	0.20
MgO	17.4	25.9	26.1	32.1	13.4	14.1	13.7	13.3	13.9	13.3	17.7	14.1	15.0
CaO	14.79	12.00	11.68	9.57	11.18	10.80	11.00	10.86	8.96	10.76	9.99	10.80	10.28
Na_2O	4.0	3.1	3.0	2.4	2.7	2.7	2.4	2.7	2.7	2.3	1.9	2.7	2.3
K_2O	2.20	1.76	1.74	1.48	1.63	1.63	1.47	1.62	1.65	1.53	1.12	1.63	1.44
P_2O_5	1.15	0.77	0.64	0.48	0.78	0.70	0.69	0.67	0.32	0.74	0.64	0.70	0.65
Total	100.69	101.19	100.26	101.94	99.89	100.11	99.77	98.07	98.13	97.24	97.73	100.11	97.95
NBO/*T*	2.28	2.50	2.54	2.90	1.63	1.60	1.56	1.65	1.62	1.59	1.85	1.60	1.62
V (ppm)	237	181	172	183	320	289	179	270	230	288	261	289	280
Cr	95	173	170	209	475	423	275	387	355	351	355	423	382
Mn	1915	1770	1600	1755	2142	1960	1477	1842	1360	1357	1600	1960	1375
Co	0.77	0.65	0.66	0.94	1.31	1.16	1.02	1.42	1.4	1.08	1.06	1.16	1.23
Ni	0.83	1	1.14	1.47	1.01	0.97	0.9	1.45	2.1	0.76	0.98	0.97	1.91
Cu	7	5.5	6.2	7.6	5.3	5.2	4.6	9.45	8.0	2.6	8.8	3.9	4.46
Zn	75.2	71	74	68.2	142	125	115	116	95	111	112	125	111
Ga	19.6	23.6	18	15.7	26.3	29.4	116	192.6	80	169	12.9	29.4	16
Sn	0.64	0.38	0.27	0.28	0.89	1.11	0.94	1.65	–	1.07	1.02	1.11	1.15
W	2.19	0.5	0.57	0.41	0.27	8.49	90.6	0.16	2.6	0.25	4.11	8.49	0.82
Mo	118	35	37.5	32.6	4.5	6.1	8.7	10.9	8.0	10.6	11.4	6.1	5.7

$Mg_2SiO_4 + O_2 = 2MgO + Fe_2SiO_4$ and one might expect to find zoned metal or olivine. However, the olivines are not compositionally zoned, indicating that equilibrium has been attained (see Table S1). Metals, although not expected to show zoning since they are simply Fe–Mo alloys, were also homogeneous. Third, experiments 25, 24, 3 and 22 define a time series carried out at 30, 60, 90 and 120 min, respectively, at 1.0 GPa and 1600 °C. After 60 min, the *D*s do not change (within error of measurements) and the system has equilibrated (Fig. S1,

Table 2
Summary table of quenched metallic liquid compositions and partition coefficients.

Sample	Cow 10	Cow 12	Cow 17	Cow 16	Cow 1	Cow 3	Cow 8	Cow 20	Cow 28	Cow 25	Cow 24	Cow 3	Cow 22
T (°C)	1500	1600	1700	1800	1500	1600	1700	1800	1900	1600	1600	1600	1600
Capsule	MgO	MgO	MgO	MgO	C	C	C	C	C	C	C	C	C
Metal													
S	–	–	–	–	0.00	0.01	0.00	–	–	–	–	0.01	–
P	0.04	0.18	0.35	0.35	0.11	0.12	0.09	0.20	0.11	0.09	0.05	0.12	0.07
Fe	95.18	95.35	95.30	95.75	89.10	90.37	89.88	89.38	90.62	90.11	89.89	90.37	90.79
Mo	3.17	2.86	2.76	2.48	3.26	2.34	2.71	2.34	2.66	2.77	2.39	2.34	2.18
C	–	–	–	–	4.5(0.8)	6.2(0.9)	5.3(1.3)	5.4(1.1)	5.5(0.7)	5.6(0.8)	5.8(0.6)	6.2(0.9)	5.2(0.7)
X_C	0.000	0.000	0.000	0.000	0.19(2)	0.24(2)	0.21(3)	0.22(3)	0.21(2)	0.22(2)	0.23(2)	0.24(2)	0.21(2)
Total	98.39	98.39	98.42	98.58	97.18	99.24	98.19	97.53	98.89	98.79	98.36	99.24	98.45
V (ppm)	5	8	11	19	41	59	63	65	138	54	78	59	73
Cr	27	22	31	48	103	100	99	134	252	81	97	100	114
Mn	49	110	150	269	59	96	98	55	198	155	239	96	133
Co	198	187	188	212	198	180	148	184	216	168	163	180	159
Ni	870	800	800	837	759	725	599	832	960	650	605	725	625
Cu	281	230	228	269	115	88	103	155	133	46	174	88	91
Zn	36	71	78	90	17	29	30	28	528	24	24	29	32
Ga	24.6	21.5	23.2	30	6.6	8.4	7.7	13	22	6.8	7.9	8.4	8.7
Sn	165	160	100	106	156	148	95	160	92	90	86	148	91
W	6.9	2.4	4.5	3.7	3.8	135	1650	4	182	4.6	81	135	17.2
Partition coefficients													
D(V)	0.021	0.044	0.064	0.10	0.13	0.20	0.35	0.24	0.60	0.19	0.30	0.20	0.26
D(Cr)	0.28	0.13	0.18	0.23	0.22	0.24	0.36	0.35	0.71	0.23	0.28	0.24	0.30
D(Mn)	0.026	0.062	0.094	0.15	0.028	0.049	0.066	0.030	0.15	0.11	0.15	0.049	0.10
D(Co)	260	290	285	225	151	155	145	130	154	123	141	155	118
D(Ni)	1050	800	700	570	750	750	670	570	457	378	356	750	296
D(Cu)	40	42	37	36	22	17	22	16	16.6	7.7	13.9	17	12.1
D(Zn)	0.48	1.0	1.1	1.3	0.12	0.23	0.26	0.24	5.6	0.22	0.22	0.23	0.28
D(Ga)	1.3	0.91	1.3	1.9	0.25	0.29	0.066	0.067	0.28	0.03	0.5	0.29	0.44
D(Sn)	260	420	370	380	180	130	100	97	–	69	70	130	68
D(W)	3.2	4.8	7.9	9.0	14	16	18	25	70	17	18	16	20
D(Mo)	270	820	740	760	7200	3800	3100	2100	3300	1700	1900	3800	3100
D(P)	0.080	0.54	1.3	1.7	0.32	0.40	0.30	0.68	0.80	0.58	0.36	0.40	0.49

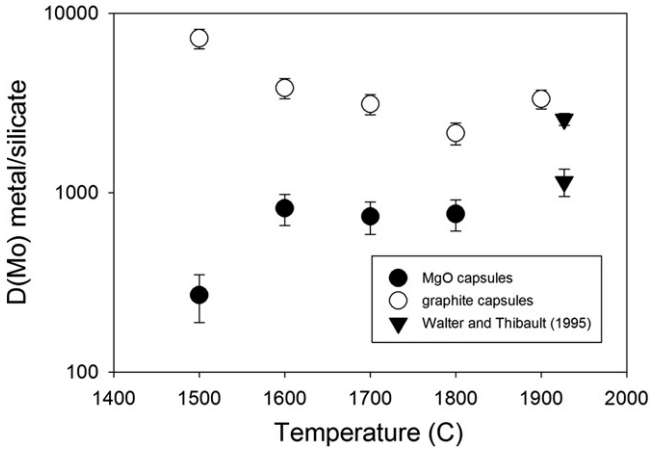

Fig. 2. $D_{Mo}^{met/sil}$ vs. temperature for both graphite and MgO capsule series. The decrease in $D_{Mo}^{met/sil}$ with temperature in the graphite series, converges towards previous results (also in graphite) at slightly higher temperatures (Walter and Thibault, 1995). The increase of $D_{Mo}^{met/sil}$ at higher temperatures in the MgO capsule series suggests that the decreasing CaO content of the melt reduces solubility of Mo in the melt. Error bars are 1σ as explained in the text.

supplementary information). Finally, the experiments reported here are longer than experiments for which time series have been done for slow diffusing elements such as W^{4+} and P^{5+}, as well and Ga^{3+} and Sn^{4+} (Righter et al., 1997; Righter and Drake, 1999, 2000).

3.2. Reaction with capsules

There were significant differences in silicate melt MgO (wt.%) with increasing temperature for the four experiments that were run in MgO capsules (Table 1). The starting material originally contained ~13% MgO but as the basalt reacted with the capsules, the amount of MgO within the sample increased to between 13 and 37 wt.% (e.g., Righter et al., 2009). The melt compositions are reproducible from experiment to experiment at any given temperature, and three analyses of different areas in the melts yielded similar results (i.e., they are homogeneous). Similarly, as mentioned already previously, the graphite capsules also reacted with the metallic portion of the starting material to form C-bearing metallic liquids. The measured C contents in the quenched metallic liquids were 4.5 to 6.2 wt.%, which corresponds to $X_C = 0.22$ (± 0.03).

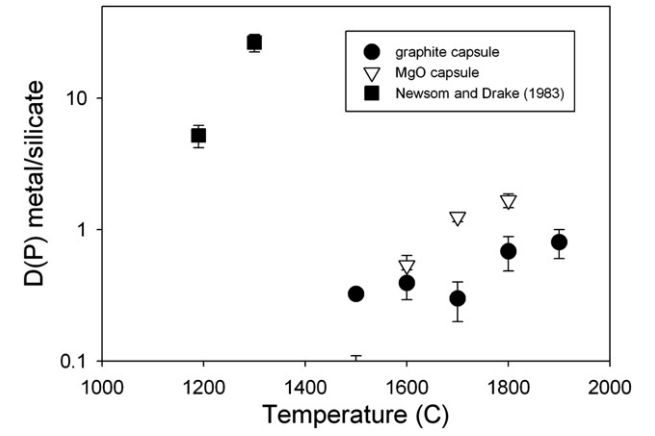

Fig. 3. Plot showing a comparison of $D_P^{met/sil}$ from three data sets. The three series include experiments run in graphite capsules, experiments run in MgO capsules and the two data points from a study by Newsom and Drake (1983). Error bars are 1σ as explained in the text.

3.3. Oxygen fugacity

Oxygen fugacity (fO_2) is also necessary to take into consideration because the partition coefficients can be sensitive to fO_2 changes. Oxygen fugacity for each experiment was calculated relative to the IW buffer, using the relation $\Delta IW = -2^*\log(X_{Fe}/X_{FeO})$, which is used in many studies of metal–silicate partitioning, and in this study ranged from 1.4 to 1.8 logfO_2 units below the iron–wüstite buffer (Table 1). For the regression calculations (see below), absolute oxygen fugacity is utilized, and calculated according to the relation $\Delta IW = -2^*\log(a_{Fe}/a_{FeO})$, where oxygen fugacity for the IW buffer at P and T was calculated using the expression of Righter et al. (1997), the activity of Fe in metal (using Swartzendruber et al., 1991 for the FeNi system) and the activity of FeO in the glass (from Holzheid et al., 1997).

4. Discussion

4.1. Partition coefficients

Because this study focused on Mo and P, we will discuss the new results for these two elements in detail, and then discuss results for all elements as a function of temperature and silicate melt composition. Differences in absolute value of D(M) between the graphite capsule and MgO capsule series for some of the elements can be attributed to variables such as fO_2 or metallic liquid content, and thus direct comparison of these two series will not allow isolation of any specific variable. In order to isolate the effects of T and melt composition we will correct the D(M) in both series as described further below.

4.1.1. Molybdenum

Walter and Thibault (1995) studied $D_{Mo}^{met/sil}$ with peridotitic or chondritic silicate melts at high PT and found a strong dependence upon silicate melt composition and oxygen fugacity, but only weak dependence on temperature and pressure. More recently, Eggins and O'Neill (2002) studied the effect of silicate melt composition on Mo solubility in silicate melts, and found a strong dependence on melt composition, as well as a specific enhancement in solubility with CaO content. Several other studies have included Mo as an element of interest (Walker et al., 1993; Hillgren et al., 1996; Righter et al., 1997), but have not been focused on the systematics of one specific variable or variables, or have studied Mo solubility with pure Mo metal (Agee and Martin, 2007), not an FeNi liquid as is relevant to Earth.

Our new results for $D_{Mo}^{met/sil}$ indicate two different trends, depending on the capsule composition. The graphite capsule experiments show that $D_{Mo}^{met/sil}$ decreases with temperature and seems consistent with the results of Walter and Thibault (1995), who also carried out with graphite capsules in a similar temperature range (Fig. 2). The MgO capsule series, on the other hand, exhibits an increase on $D_{Mo}^{met/sil}$ with temperature, also converging with the results of Walter and Thibault (1995), and suggests that melt compositional changes (increasing MgO) cause an increase in $D_{Mo}^{met/sil}$. The convergence with Walter and Thibault (1995) experiments is also expected because they used peridotite silicate melts like our highest temperature experiments in the MgO series. This will be discussed in more detail below.

4.1.2. Phosphorus

The effect of T and fO_2 metal–silicate partitioning of P has been studied by Newsom and Drake (1983). The effects of sulfur and carbon in the metal phase were investigated by Jana and Walker (1997a,b), and melt compositional effects were evident from the datasets of Young et al. (1992) and Pak and Fruehan (1986), but the latter were focused on slag silicate melt compositions that are not necessarily transferable to the molten early Earth compositions. Our $D_P^{met/sil}$ results from the nine experimental runs that were analyzed for this study are compared to the results of a study done by Newsom and

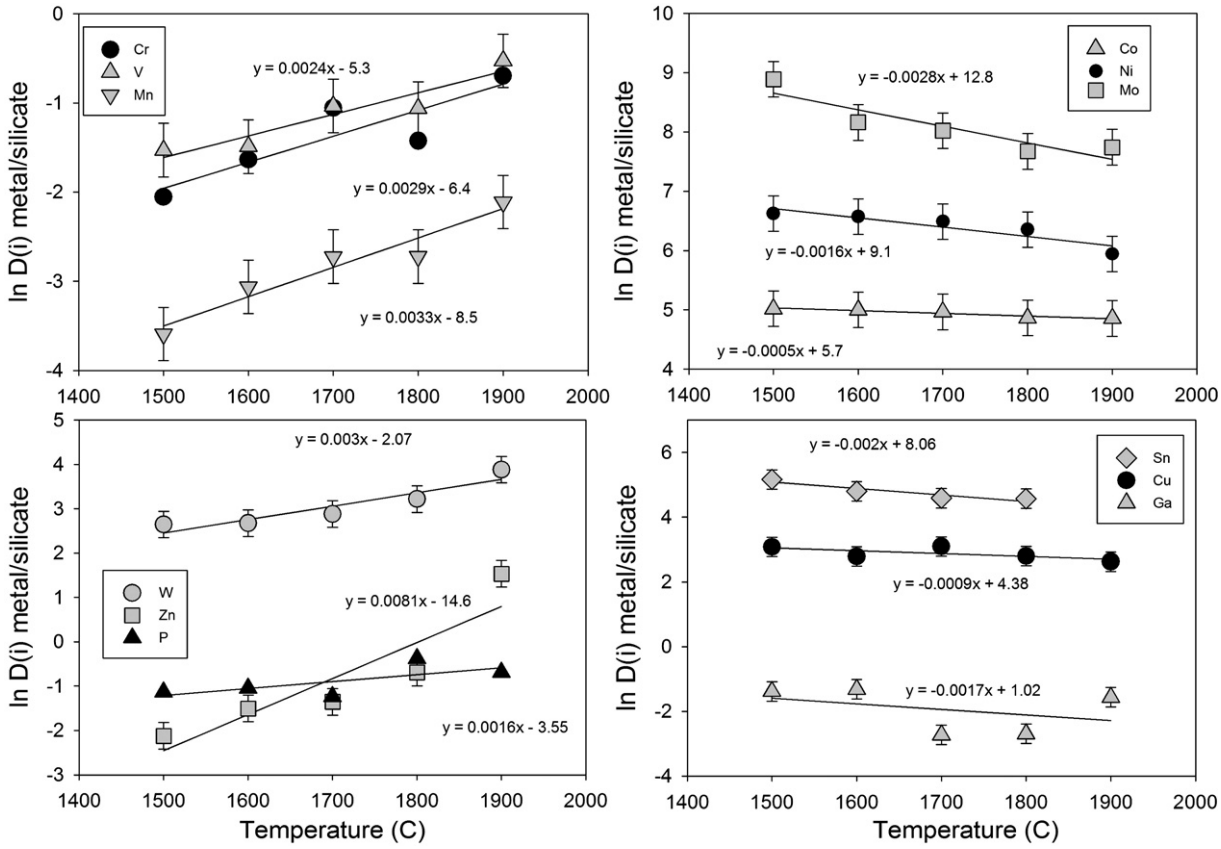

Fig. 4. ln$D$(i) metal/silicate vs. temperature (°C) for all 12 elements studied. In each case, the effect of oxygen fugacity has been normalized or corrected to the relative fO_2 of the 1500 °C experiment, as described in the text. Once this correction is made, the effect of temperature can be evaluated for each element because the pressure, fO_2, silicate and metallic melt compositions are all constant. A linear fit to each element series is shown. This fit is applied to the MgO capsule series in Fig. 5 to illustrate the effect of variable silicate melt composition. Error bars are 1σ as explained in the text.

Drake (1983) at 1190° and 1300 °C (Fig. 3). These three data sets demonstrate that increasing T will increase $D_P^{met/sil}$.

4.1.3. Other elements

The results for all other elements are split into two groups for ease of graphical display in order to highlight the differences in magnitude of D (M/S). The elements Ni, Co, Cu, Sn and W are combined (Figs. S2a and S3a, supplementary information), as are Mn, V, Cr, Ga, and Zn (Figs. S3b and S3b, supplementary information). Instead of a detailed discussion of each of these elements (as with Mo and P), the effect of temperature and melt composition on each will be discussed in the next two sections.

4.2. Effect of temperature (graphite capsule series)

The graphite capsule series of experiments was carried out at constant pressure, silicate melt composition, and metallic melt composition. The carbon contents of the metallic liquids in the graphite capsule series of experiments are in good agreement with those expected from the nearly vertical phase boundary in the Fe–C phase diagram (Dasgupta and Walker, 2008), and show that the carbon content is essentially constant in the graphite capsule series across this temperature range. The fO_2 in this series is very similar, $\Delta IW = -1.44$ to -1.56, and therefore a small correction can be applied to the results to normalize them to the same relative fO_2, that of the 1500 °C run. This is done by making a small correction to the partition coefficient by $n/4^*\Delta IW\ (T) - \Delta IW\ (1500)$, where n is the valence of the element in the silicate melt (Table S2). Once this correction is made, the graphite capsule series is suitable for examining the effect of temperature on the magnitude of D for all elements, since all other variables (pressure, silicate melt, fO_2 and metal composition) are constant (Fig. 4).

4.2.1. Molybdenum

In this study, we have isolated the effect of temperature (at fixed pressure, composition, and oxygen fugacity), and also been able to reconcile different databases by covering intervening parameter space. For example, the results of our studies between 1500 and 1900 °C show a decrease in our uncorrected $D_{Mo}^{met/sil}$ which approaches the values of $D_{Mo}^{met/sil}$ reported by Walter and Thibault (1995) at 1900–2000 °C (Fig. 2). The effect of temperature causes a decrease on the order of 5x across 400 °C (Fig. 4), the strongest decrease observed for any element in this study.

4.2.2. Tungsten

Studies of tungsten partitioning between metal and silicate melt have been extensive, with the role of oxygen fugacity (O'Neill et al., 2008), carbon in metallic liquid (Righter and Drake, 1999; Cottrell et al., 2009) and melt composition (Walter and Thibault, 1995; Cottrell et al., 2009), being identified as significant factors in controlling $D_W^{met/sil}$. In fact, some studies have emphasized that $D_W^{met/sil}$ can be understood in terms of fO_2, metallic C content, and silicate melt composition only, with the effects of variables temperature and pressure being minor or insignificant. Here we observe a clear increase in $D_W^{met/sil}$ with temperature, in stark contrast to that observed for $D_{Mo}^{met/sil}$ (Fig. 4).

4.2.3. Nickel and cobalt

The effect of fO_2 on $D_{Ni}^{met/sil}$ and $D_{Co}^{met/sil}$ metal/silicate partitioning has been studied by many, and it is clear that these two cations are dependent upon solubility into the melt as a 2+ oxide (Capobianco and Amelin, 1994; Holzheid et al., 1997). More recent work has focused on the role of temperature since some predictive expressions (e.g., Righter et al., 1997; Righter and Drake, 1999) had a significant T dependence.

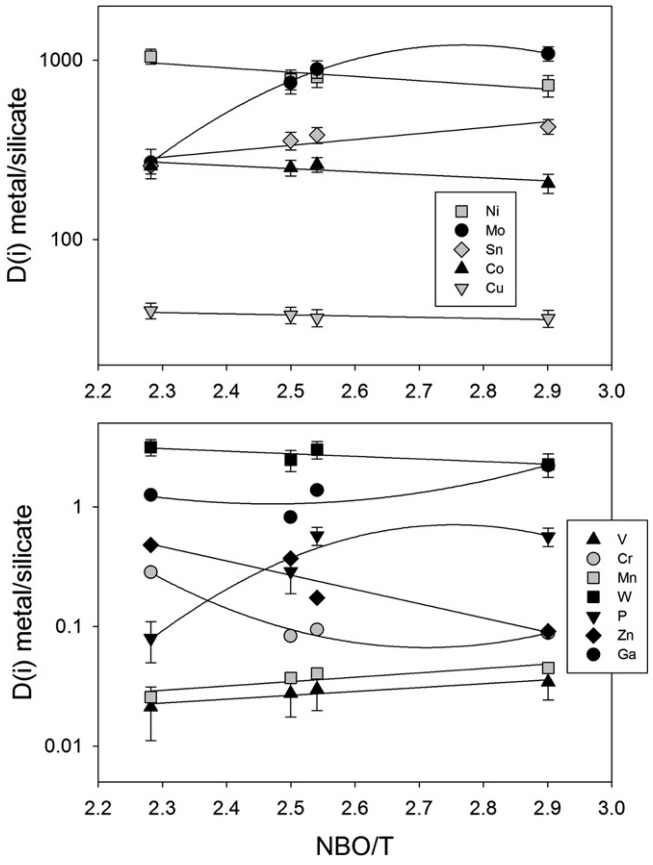

Fig. 5. D(i) metal/silicate vs. variable silicate melt structural state as monitored by the parameter NBO/T. The two sets of elements are divided between $D>10$ and $D<10$ for ease of presentation. All values plotted have been corrected for temperature by normalization to the 1500 °C experiment using the linear temperature fits from Fig. 4, as explained also in the text. Error bars are 1σ as explained in the text.

These recent studies have demonstrated a systematic but small T dependence (Chabot et al., 2005; Kegler et al., 2008). Our series of experiments provide an opportunity to evaluate those previous T studies, and we also see a small temperature dependence in $D_{Ni}^{met/sil}$ and $D_{Co}^{met/sil}$ with a clear decrease at higher temperatures (Fig. 4).

4.2.4. Manganese, vanadium, and chromium

Previous systematic studies of Mn, V, and Cr have included temperature as a variable, but had several drawbacks. First, the experiments of Gessmann and Rubie (1998) looked at the effect of temperature but instead of silicate–metallic melt partitioning, they studied metallic melt–magnesiowüstite crystal partitioning. Similarly, the study of Chabot and Agee (2003) examined temperature effects, but for a potassium feldspar composition silicate melt — far different from the peridotite composition that would have been likely had there been an early magma ocean. Our study thus represents the first look at temperature variation with silicate melts that contain FeO, MgO, and SiO_2 (and low CaO and Al_2O_3) contents more similar to those in a magma ocean. Despite the differences in melt composition, $D_V^{met/sil}$, $D_{Mn}^{met/sil}$, and $D_{Cr}^{met/sil}$ all indicate an increase with temperature (Fig. 4), in agreement with the magnitude of increases seen by Chabot and Agee (2003), who observed all three elements becoming more siderophile at high temperatures.

4.2.5. Gallium, tin, copper and zinc

Righter and Drake (2000) and other recent studies have studied Ga during metal/silicate equilibrium, but none have examined a systematic temperature variation. The series of experiments in graphite capsules exhibits an overall decrease in $D_{Ga}^{met/sil}$ over the temperature interval studied here (Fig. 4). Righter et al. (2009) presented an updated $D_{Sn}^{met/sil}$ expression based on new experimental data to combine with Capobianco et al. (1999) and Righter and Drake (2000). The expression predicts a small decrease in $D_{Sn}^{met/sil}$ with temperature, which we see here in the graphite capsule series (Fig. 4). Temperature was predicted to cause a decrease in $D_{Cu}^{met/sil}$ by Righter and Drake (2000), which was later verified by Holzheid and Lodders (2001) and Corgne et al. (2008) in separate studies of very different composition systems. Our new data also show a slight decrease in $D_{Cu}^{met/sil}$ with temperature. Finally, there is only one previous study of $D_{Zn}^{met/sil}$ by Corgne et al. (2008) and they observed a small decrease in $D_{Zn}^{met/sil}$ with increasing temperature. Here we see an increase in $D_{Zn}^{met/sil}$ with temperature (Fig. 4), contrary to the previous work.

4.2.6. Summary — effect of temperature

The metal/silicate partition coefficients for many elements exhibit either small (Co, Cu, Sn, Ga) or more significant (Mo, Ni) decreases with increasing temperature. Other elements exhibit significant increases (W, P, Zn, Mn, V, Cr) in D(met/sil) with increasing temperature. It is obviously not valid to generalize about the effects of temperature on a metal silicate partition coefficient, and the behavior of each element is determined by its specific thermochemistry in high PT molten systems.

4.3. Effect of silicate melt composition (MgO series)

Temperature effects quantified in the graphite capsule series can be used to correct for temperature in the MgO capsule series, thus isolating any melt compositional effects. The effect of temperature in the graphite series is fit with a linear relationship (Fig. 4) and then a correction applied to the MgO series. The effect of variable fO_2 is also applied to the MgO capsule series, where fO_2 varies more between runs that it does for the graphite series. Therefore the MgO series are corrected for both fO_2 and temperature, and since they are carried out at constant pressure and metallic liquid composition (Fe–Mo alloys) the corrected values (Table S2, supplementary information) allow isolation of the effect of silicate melt composition over an interval from basaltic to peridotitic melts (NBOT~2.2 to 2.9; Fig. 5). As with temperature, silicate melt composition affects some elements differently than others, as will be clear below.

4.3.1. Molybdenum

The increasingly CaO-poor and MgO-rich melts in the MgO capsule series between 1500 and 1900 °C cause $D_{Mo}^{met/sil}$ to increase (Fig. 5), consistent with what has been predicted for Mo solubility by Eggins and O'Neill (2002). The effect on Mo is a factor of 5 across the melt compositional range studied here (Fig. 5).

4.3.2. Phosphorus

A strong melt compositional effect on $D_P^{met/sil}$ was proposed previously by Righter (2003), and can be seen by comparison of our new results with those of Newsom and Drake (1983) (Fig. 3). Their results at low pressure and comparable T and fO_2, are much higher than ours where there is overlap of these variables, indicating that the peridotitic compositions dissolve more P than the basaltic eucrites used by Newsom and Drake (1983). However, based on our data, $D_P^{met/sil}$ can increase by as much as a factor of 10 across this melt compositional range (Fig. 5). This increase may reflect the higher MgO contents of the melts (and lower CaO contents).

4.3.3. Tungsten

We see a very minimal melt compositional effect on $D_W^{met/sil}$. In fact, we see a slight decrease in $D_W^{met/sil}$ in the MgO series (Fig. 5). This is a surprising observation given that several previous studies have examined melt compositional dependence, and found strong compositional dependence (e.g., Walter and Thibault, 1995). There are clearly differences in the activities of WO_2 in Ca vs. Mg-bearing melts (O'Neill et al., 2008), and it is likely these factors have influenced

previous interpretations of a strong compositional influence. However, our results indicate that melt compositional effects (Fig. 5) may be less important than temperature (Fig. 4).

4.3.4. Nickel and cobalt

Some previous studies also focused on the role of silicate melt composition in controlling $D_{Ni}^{met/sil}$ and $D_{Co}^{met/sil}$, and found that $D_{Ni}^{met/sil}$ and $D_{Co}^{met/sil}$ are barely different if the silicate melt is potassium feldspar vs. peridotite (Chabot et al., 2005). Our results however, demonstrate a small, but nonetheless significant effect of melt compositions, from basalt to peridotite (Fig. 5), which was also suggested in the study of Eggins and O'Neill (2002). $D_{Ni}^{met/sil}$ and $D_{Co}^{met/sil}$ are lower in the experiments in which there is peridotite melt (32 wt.% MgO) present as opposed to basaltic melt (15 wt.% MgO). Therefore silicate melt composition cannot be ignored when applying partitioning results to planetary differentiation.

4.3.5. Manganese, vanadium, and chromium

The effect of melt composition on these three elements is mixed, in contrast to the effect of temperature which is similar for each element. For example, $D_{Mn}^{met/sil}$ and $D_{V}^{met/sil}$ exhibit a clear increase in more peridotite-like melts (Fig. 5), whereas $D_{Cr}^{met/sil}$ exhibits a decrease. Previous studies have concluded that melt composition does not have a strong effect on these three elements (Chabot and Agee, 2003). But their predicted values are in poor agreement with our results, indicating that those expressions may have been heavily influenced by the experiments with potassium feldspar melt composition. In contrast, the predictions of Wood et al. (2008) for $D_{Cr}^{met/sil}$ and $D_{V}^{met/sil}$ are in better agreement with our results, and their expressions are calibrated for peridotite liquids.

4.3.6. Gallium, tin, copper, and zinc (volatile elements)

Our results for $D_{Ga}^{met/sil}$ show a small increase for more peridotite-like melts, increasing from values near one to slightly greater than 1 (Fig. 5). Similarly, our results show little to no change in $D_{Cu}^{met/sil}$ with melt composition (Fig. 5). On the other hand, there is a clear increase in $D_{Sn}^{met/sil}$ in the MgO capsule series that indicates a melt compositional effect (Fig. 5). And $D_{Zn}^{met/sil}$ decreases slightly with melt composition (Fig. 5). Despite the differences for Zn between this study and Corgne et al. (2008), the values of $D_{Zn}^{met/sil}$ in both studies suggest that the depletion of Zn in the Earth's mantle, 0.075 relative to CI and Mg (McDonough and Sun, 1995), can be explained by the volatility of Zn rather than siderophile behavior at high pressure and temperature.

4.3.7. Summary — melt composition

As with temperature, the effects of melt composition seem to be specific to each element, without a clear basis for making generalizations due to factors such as cation charge. For example, our data show evidence for melt depolymerization causing increases in D(met/sil) for Ga, P, Mn, V, Sn, and Mo. These elements dissolved into silicate melts as 2+, 3+, 4+ and 5+. At the same time, we see evidence for melt depolymerization causing a decrease in D(met/sil) for W, Zn, Cr, Ni, Co and Cu (Fig. 5). Again, these elements have valences ranging from 2+, 3+, and 4+. There has been much work done on CaO-bearing melts and the effects of melt composition evaluated using NBO*T*. However, MgO-rich vs. CaO-rich melts, although both exhibiting similar NBO*T* values, may have very different chemical activity effects and thus application to peridotite magma ocean scenarios must be carried out with MgO-rich melts. The decreasing D(met/sil) seen for W, Zn, Cr, Ni, Co, and Cu may illustrate an overall affinity for MgO-rich basic melts compared to Mo, P, Mn, Sn, and V.

4.4. Application to the Earth: Mo and P

Metal–silicate partition coefficients for siderophile elements for a terrestrial planet growing during core formation will change as a function of pressure, temperature, oxygen fugacity, and metal and silicate composition. Calculation of metal–silicate partition coefficients as a function of all these variables have been possible using an approach guided by chemical thermodynamics where:

$$\ln D(\text{met/sil}) = a\ln fO_2 + b/T + cP/T + d(1-X_S) + e(1-X_C) + f[S] + \sum g_i X_i + h \quad (1)$$

The *a*, *b*, *c*, and *h* terms relate to valence, enthalpy (H/RT), volume (VP/RT), and entropy (S/R), respectively, the *d* and *e* terms relate to activity expressions for these elements in a metallic liquid (X_S and X_C = mole fraction of S and C in the metallic liquid, respectively), and the f term relates to the S content of the silicate melt.

The g terms relate to silicate melt structure and have sometimes been regressed against NBO*T*, as defined by Mysen (1991) and Mills (1993) (e.g., Walter and Thibault, 1995; Righter et al., 1997), but it has become clear that this term is not a completely satisfactory parameter in gauging melt compositional effects. CaO and MgO, for example, both network modifiers, have differing effects on D (e.g., Eggins and O'Neill, 2002), and this is an important distinction to make because the mantle is dominated by MgO. Instead the melt compositional effects can be monitored using simple oxide mole fractions — X_{SiO_2}, X_{MgO}, X_{CaO}, X_{Al_2O3}, and X_{FeO} — as has been done by Righter and Drake (1999). The oxide mole fraction approach works well if there are many data across a wide compositional range with which to calibrate, and in the case of P there are ~100 experiments.

4.4.1. Molybdenum

The coefficients a through g in Eq. (1) are derived by multiple linear regression of experimental database (Table S3, supplementary information). Comparison of calculated (using Eq. (1)) to measured $D_{Mo}^{met/sil}$ for 65 experiments shows good agreement (Fig. S4, supplementary information), with a few exceptions. The coefficient associated with fO_2 (a) is −1.14, which is consistent with the valence of Mo being dominated by 4+, but having some small additional component of 6+ (Table S3, supplementary information). The regression coefficients predict a strong decrease in $D_{Mo}^{met/sil}$ with pressure, but only a slight decrease with temperature, consistent with our graphite capsule results. The effect of metallic liquid C content is to increase $D_{Mo}^{met/sil}$, while S content reduced the magnitude of $D_{Mo}^{met/sil}$, both consistent with previous studies (e.g., Hillgren, 1993; Jana and Walker, 1997b).

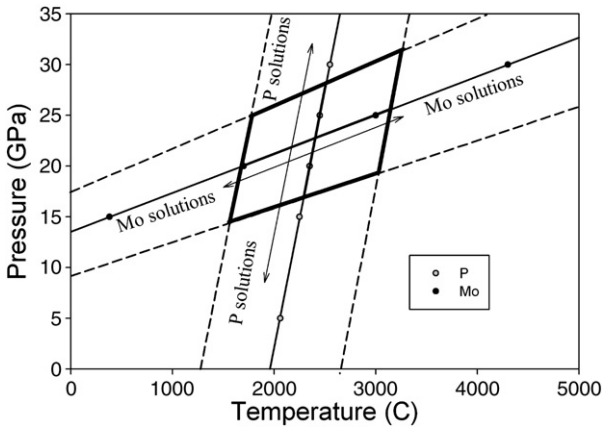

Fig. 6. Pressure–temperature conditions where $D_P^{met/sil} = 5$ and $D_{Mo}^{met/sil} = 42$ for calculated using regression coefficients from Table 5 and for conditions of fixed mantle composition, metallic liquid contents of $X_S = 0.05$ and $X_C = 0.1$, and oxygen fugacity of $\Delta IW = -2$. The curves for Mo and P cross near 22.5 GPa and 2400 °C, but the full range of possible solutions, defined by the error on the partition coefficient calculations, is from 15 to 32 Ga, and 1700 to ~3000 °C.

4.4.2. Phosphorus

Phosphorus partition coefficients $D_P^{met/sil}$ in this study can be combined with previous results (Newsom and Drake, 1983; Schmitt et al., 1989; Young et al., 1992; Walker et al. 1993; Hillgren, 1993; Hillgren et al., 1996; Righter et al., 1997; Jana and Walker, 1997a,b; Righter and Drake, 1999, 2000). The studies of Newsom and Drake (1983) and Schmitt et al. (1989) and Hillgren (1993) cover the effects of fO_2 and temperature at one bar. The high pressure studies of Walker et al. (1993), Hillgren et al. (1996), Righter and Drake (2000) and this study help to constrain the effects of pressure. The Jana and Walker (1997a) and Young et al. (1992) were done with variable melt compositions. And finally the experiments of Hillgren (1993), Jana and Walker (1997b), Righter and Drake (2000), and this study constrain the roles of S and C. The f term for sulfur content of the silicate melt was dropped from the expression for $D_P^{met/sil}$ because it was insignificant in regressions in which it was included (Fig. S5 and Table S3, supplementary information).

4.4.3. Mantle concentrations and D required for equilibrium

Mantle siderophile element (i) concentrations resulting from core formation depend upon several factors: the initial siderophile element concentration of the bulk planet, core size, and the magnitude of the metal–silicate partition coefficient (e.g., Righter, 2003). These three factors can be combined to quantify the content of a planetary mantle after core formation. The expression determining the concentration of a siderophile element in a planet's mantle is (from mass balance constraints):

$$C_{sil}^{i} = \frac{C_{bulk}^{i}}{[x + (1-x)(D_{met/sil}^{i})]} \quad (2)$$

where x is the silicate fraction of the planet; C_{sil}^{i} and C_{bulk}^{i} are concentrations of i in the magma ocean and bulk planet, respectively; and $D_{met/sil}^{i}$ is calculated using an equation such as presented in the manuscript for siderophile elements Mo and P. Eq. (2) can be used to calculate the concentration of a siderophile element in a magma ocean after core formation, or it can be used to constrain the magnitude of D required to explain a known mantle siderophile content, assuming one has independent estimates of the core size and bulk composition.

Application of the results for Mo and P can be made to the Earth. Using Eq. (2) and assuming a bulk Earth composition of CI chondrites, and a core that is 32 mass % of the planet, the required D(met/sil) to produce a mantle Mo content of 65 ppb and mantle P content of 95 ppm are 42 and 5, respectively (from McDonough and Sun, 1995; Sims et al., 1990). The calculation for P assumes a factor of 5 volatility correction according to the volatility trend of McDonough and Sun (1995). Fixing the silicate melt composition at that of the primitive mantle (McDonough and Sun, 1995), the core metal content at $X_S = 0.05$ and $X_C = 0.10$, the oxygen fugacity of $\Delta IW = -2$, and the sulfur content of the silicate melt at 200 ppm, the P and T at which $D_{Mo}^{met/sil}$ and $D_P^{met/sil}$ attain these values can be calculated in PT space (Fig. 6). If these two separate curves cross, it indicates a region of PT space where these two elements can be satisfied by metal–silicate equilibration. As one can see from the resulting calculations, both Mo and P concentrations in the terrestrial mantle can be explained by a metal–silicate equilibration at pressures between 15 to 32 GPa and 1700 to 3000 °C. The range of values results from consideration of the error on the calculation partition coefficients (Fig. 6). The two curves cross at 22.5 GPa and 2400 °C; these conditions are those of a relatively shallow magma ocean compared to the more extreme conditions proposed by recent models of up to 50 GPa and 4000 °C (Wade and Wood, 2005; Wood et al., 2008). In summary, these results for Mo are consistent with the idea that the Earth experienced a hot early differentiation event.

5. Summary

We have studied the partitioning behavior of Mo, P, and ten other siderophile elements, at variable temperatures and silicate melt compositions including peridotitic liquids. The last decade has seen a large increase in publication of metal–silicate partitioning data for siderophile elements, and a generally stated conclusion is that high temperature conditions make siderophile elements less siderophile. However, our findings are that half of these elements become more siderophile at high temperatures. This is consistent with the prediction of Capobianco et al. (1993) in which increases in D(met/sil) with temperature were predicted based on the van't Hoff equation.

In addition, it is clear that there are strong silicate melt compositional effects on partition coefficients. Melt composition must be quantified in predictive expressions. In many cases, a simple or single melt term is not adequate, and richer terms that capture melt structural and compositional differences between aluminosilicate and peridotite melts, for example, are required.

Finally, the results for Mo and P are combined with previous studies to show that the concentrations of these two elements in the mantle of the Earth are consistent with an early high temperature melting event. However, for Mo, the coverage in pressure–temperature space is not nearly as extensive as elements like Ni and Co, so much work remains to explore high pressure effects on this important refractory siderophile element.

Acknowledgements

K. Acuff (Pando) was supported by a summer internship at the Lunar and Planetary Institute (LPI). The research was supported by an RTOP to K. Righter and a Packard Fellowship to C.-T. Lee. M. Pertermann and M. Righter provided assistance with the LA-ICP-MS analysis, as did A. Peslier and L. Le on the electron microprobe at JSC. The manuscript was substantially improved by the reviews of P. Kegler and another anonymous journal reviewer.

Appendix A. Supplementary data

Supplementary data associated with this article can be found, in the online version, at doi:10.1016/j.epsl.2009.12.018.

References

Agee C.B. and Martin, E. (2007) Molybdenum Solubility in Silicate Melt at High Pressures and Temperatures: Experimental Constraints on Planetary Core Formation. LPS XXXVII, abstract # 2170.
Agrinier, A., Lee, C.-T., 2007. Quantifying trace element disequilibria in mantle xenoliths and abyssal peridotite. Earth Planet. Sci. Lett. 257, 290–298.
Campbell, A.J., Humayun, M., 2005. Compositions of group IVB iron meteorites and their parent melt. Geochim. Cosmochim. Acta 69, 4733–4744.
Capobianco, C.J., Amelin, A.A., 1994. Metal–silicate partitioning of nickel and cobalt: the influence of temperature and oxygen fugacity. Geochim. Cosmochim. Acta 58, 125–140.
Capobianco, C.J., Jones, J.H., Drake, M.J., 1993. Metal–silicate thermochemistry at high temperature: magma oceans and the "excess siderophile element" problem of the Earth's upper mantle. J. Geophys. Res. 98 (E3), 5433–5443.
Capobianco, C.J., Drake, M.J., DeAro, J., 1999. Siderophile geochemistry of Ga, Ge, and Sn: cationic oxidation states in silicate melts and the effect of composition in iron–nickel alloys. Geochim. Cosmochim. Acta 64, 3581–3597.
Chabot, N.L., Agee, C.B., 2003. Core formation in the Earth and Moon: new experimental constraints from V, Cr, and Mn. Geochim. Cosmochim. Acta 67, 2077–2091.
Chabot, N.L., Draper, D.S., Agee, C.B., 2005. Conditions of core formation in the Earth: constraints from nickel and cobalt partitioning. Geochim. Cosmochim. Acta 69, 2141–2151.
Corgne, A., Keshav, S., Wood, B.J., McDonough, W.F., Fei, Y., 2008. Metal–silicate partitioning and constraints on core composition and oxygen fugacity during Earth accretion. Geochim. Cosmochim. Acta 72, 574–589.
Cottrell, E., Walter, M.J., Walker, D., 2009. Metal–silicate partitioning of tungsten at high pressure and temperature: implications for equilibrium core formation in Earth. Earth Planet. Sci. Lett. 281, 275–287.
Dasgupta, R., Walker, D., 2008. Carbon solubility in core melts in a shallow magma ocean environment and distribution of carbon between the Earth's core and the mantle. Geochim. Cosmochim. Acta 72, 4627–4641.

Eggins, S.M., O'Neill, H.St.C., 2002. The effect of melt composition on trace element partitioning: an experimental investigation of the activity coefficients of FeO, NiO, CoO, MoO_2 and MoO_3 in silicate melts. Chem. Geol. 186, 151–181.
Filiberto, J., Treiman, A.H., Le, L., 2008. Crystallization experiments on a Gusev basalt composition. Meteorit. Planet. Sci. 43, 1137–1146.
Gao, S., Liu, X.M., Yuan, H.L., Hattendorf, B., Gunther, D., Chen, L., Hu, S.H., 2002. Determination of forty two major and trace elements in USGS and NIST SRM glasses by laser ablation-inductively coupled plasma-mass spectrometry. Geostand. Newsl. — J. Geostand. Geoanal. 26, 181–196.
Gessmann, C.K., Rubie, D.C., 1998. The effect of temperature on the partitioning of nickel, cobalt, manganese, chromium, and vanadium at 9 GPa and constraints on formation of the Earth's core. Geochim. Cosmochim. Acta 62, 867–878.
Hillgren V.J. (1993) Partitioning Behavior of Moderately Siderophile Elements in Ni-rich Systems: Implications for the Earth and Moon. PhD Thesis. Univ. Ariz. 423 pp.
Hillgren, V.J., Drake, M.J., Rubie, D.C., 1996. High pressure and high temperature metal–silicate partitioning of siderophile elements: the importance of silicate liquid composition. Geochim. Cosmochim. Acta 60, 2257–2263.
Holzheid, A., Lodders, K., 2001. Solubility of copper in silicate melts as a function of oxygen and sulfur fugacities, temperature, and silicate composition. Geochim. Cosmochim. Acta 65, 1933–1951.
Holzheid, A., Palme, H., Chakraborty, S., 1997. The activities of NiO, CoO and FeO in silicate melts. Chem. Geol. 139, 21–38.
Jana, D., Walker, D., 1997a. The influence of silicate melt composition on distribution of siderophile elements among metal and silicate liquids. Earth Planet. Sci. Lett. 150, 463–472.
Jana, D., Walker, D., 1997b. The influence of sulfur on partitioning of siderophile elements. Geochim. Cosmochim. Acta 61, 5255–5277.
Kegler, Ph., Holzheid, A., Frost, D.J., Rubie, D.C., Dohmen, R., Palme, H., 2008. New Ni and Co metal–silicate partitioning data and their relevance for an early terrestrial magma ocean. Earth Planet. Sci. Lett. 268, 28–40.
Lewis, R.D., Lofgren, G.E., Franzen, H.F., Windom, K.E., 1993. The effect of Na vapor on the Na content of chondrules. Meteorites 28, 622–628.
Li, J., Agee, C.B., 1996. Geochemistry of mantle–core formation at high pressure. Nature 381, 686–689.
McDonough, W.F., Sun, S.-s., 1995. Composition of the Earth. Chem. Geol. 120, 223–253.
Mills, K.C., 1993. The influence of structure on the physico–chemical properties of slags. ISIJ Int. 33, 148–155.
Mysen, B.O., 1991. Volatiles in magmatic liquids. In: Perchuk, L.L., Kushiro, I. (Eds.), Physical Chemistry of Magma. Cambridge University Press, New York, pp. 435–476. Ch. 16.
Newsom, H.E., Drake, M.J., 1983. Experimental investigations of the partitioning of phosphorus between metal and silicate phases: implications for the Earth, Moon and eucrite parent body. Geochim. Cosmochim. Acta 47, 93–100.
Ohtani, E., Yurimoto, H., Seto, S., 1997. Element partitioning between metallic liquid, silicate liquid, and lower-mantle minerals: implications for core formation of the Earth. Phys. Earth Planet. Inter. 100, 97–114.
O'Neill, H., St, C., Berry, A.J., Eggins, S.M., 2008. The solubility and oxidation state of tungsten in silicate melts: implications for the comparative chemistry of W and Mo in planetary differentiation processes. Chem. Geol. 255, 346–359.
Pak, J.J., Fruehan, R.J., 1986. Soda slag system for hot metal dephosphorization. Met. Trans. 17B, 797–804.
Righter, K., 2003. Metal–silicate partitioning of siderophile elements and core formation in the early Earth and terrestrial planets. Annu. Rev. Earth Planet. Sci. 31, 135–174.
Righter, K., Drake, M.J., 1999. Effect of water on metal–silicate partitioning of siderophile elements: a high pressure and temperature terrestrial magma ocean and core formation. Earth Planet. Sci. Lett. 171, 383–399.
Righter, K., Drake, M.J., 2000. Metal/silicate equilibrium in the early Earth: new constraints from the volatile moderately siderophile elements Ga, Cu, P and Sn. Geochim. Cosmochim. Acta 64, 3581–3597.
Righter, K., Drake, M.J., Yaxley, G., 1997. Prediction of siderophile element metal–silicate partition coefficients to 20 GPa and 2800 °C: the effect of pressure, temperature, fO_2 and silicate and metallic melt composition. Phys. Earth Planet. Inter. 100, 115–134.
Righter, K., Sutton, S.R., Newville, M., Le, L., Schwandt, C.S., Uchida, H., Lavina, B., Downs, R.T., 2006. Oxidation state of vanadium in spinel and silicate melt: implications for planetary basalts and mantle melting. Am. Mineral. 91, 1643–1656.
Righter, K., Humayun, M., Campbell, A.J., Danielson, L.R.D., Hill, D., Drake, M.J., 2009. Experimental studies of metal–silicate partitioning of Sb: Implications for the terrestrial and lunar mantles. Geochim. Cosmochim. Acta 73, 1487–1504.
Rubie, D.C., Melosh, H.J., Reid, J.E., Liebske, C., Righter, K., 2003. Mechanisms of metal–silicate equilibration in the terrestrial magma ocean. Earth Planet. Sci. Lett. 205, 239–255.
Schmitt, W., Palme, H., Wanke, H., 1989. Experimental determination of metal/silicate partition coefficients for P, Co, Ni, Cu, Ga, Ge, Mo, W and some implications for the early evolution of the Earth. Geochim. Cosmochim. Acta 53, 173–186.
Sims, K.W.W., Newsom, H.E., Gladney, E.S., 1990. In: Newsom, H.E., Jones, J.H. (Eds.), The Origin of the Earth. Chemical Fractionation During Formation of the Earth's Core and Continental Crust: Clues From As, Sb, W and Mo. Oxford Univ. Press, New York, pp. 291–318.
Swartzendruber, L.J., Itkin, V.P., Alcock, C.B., 1991. The Fe–Ni (iron–nickel) system. J. Phase Equilib. 12, 288–312.
Toplis, M.J., 2005. The thermodynamics of iron and magnesium partitioning between olivine and liquid: criteria for assessing and predicting equilibrium in natural and experimental systems. Contrib. Mineral. Petrol. 149, 22–39.
Wade, J., Wood, B.J., 2001. Earth's 'missing' niobium may be in the core. Nature 409, 75–78.
Wade, J., Wood, B.J., 2005. Core formation and the oxidation state of the Earth. Earth Planet. Sci. Lett. 236, 78–95.
Walker, D., Norby, L., Jones, J.H., 1993. Superheating effects on metal–silicate partitioning of siderophile elements. Science 262, 1858–1861.
Walter, M.J., Thibault, Y., 1995. Partitioning of tungsten and molybdenum between metallic liquid and silicate melt. Science 270, 1186–1189.
Walter, M.J., Newsom, H., Ertel, W., Holzheid, A., 2000. Siderophile elements in the Earth and Moon: metal/silicate partitioning and implications for core formation. See Canup & Righter 2000, pp. 265–290.
Wood, B.J., Wade, J., Kilburn, M., 2008. Core formation and the oxidation state of the Earth: additional constraints from Nb, V and Cr partitioning. Geochim. Cosmochim. Acta 72, 1415–1426.
Young, R.W., Duffy, J.A., Hassall, G.J., Xu, Z., 1992. Use of optical basicity concept for determining phosphorus and sulphur slag–metal partitions. Ironmak. steelmak. 19, 201–219.